Progress Report

RETROFIT CATHODIC PROTECTION OF MARINE PIPELINES ASSOCIATED WITH PETROLEUM PRODUCTION

submitted to

Minerals Management Service
Department of the Interior

prepared by

Dr. William H. Hartt, Professor and Director
Center for Marine Materials
Department of Ocean Engineering
Florida Atlantic University – Sea Tech Campus
101 North Beach Road
Dania Beach, Florida 33004

May 18, 2000

TECHNICAL SUMMARY

Marine oil and gas transportation pipelines have been in service in the Gulf of Mexico for almost 50 years. These lines are invariably protected from external corrosion by a combination of coatings and cathodic protection (cp); however, the design life of such protection systems upon older lines has now been exceeded in many cases and retrofitting may soon be required. This project was initiated in 1997 for the purpose of establishing criteria and protocols for design of pipeline retrofit cp systems. This report describes progress that has been made to-date although the research remains ongoing. The building block of the study has been development of a first-principles based equation that projects potential attenuation and anode current output for a cp system comprised of multiple galvanic anodes. This equation incorporates all relevant terms, including 1) anode (electrolyte) and metallic path resistances, 2) coating quality, 3) pipe current density demand, 4) pipe and anode dimensions, and 5) electrolyte properties. This is in contract to previous approaches, including the equations of Morgan and Uhlig and Boundary Element Modeling computer programs, which exclude one or more of these terms. Accuracy and utility of the equation with regard to projection of 1) potential profiles, 2) anode current output, and 3) current density demand (a parameter that is critical to retrofit cp design) has been demonstrated. Also important is the fact that maximized spacing of anode sleds (such sleds are invariably a part of pipeline cp retrofits) can be projected from the equation, whereas none of the existing alternative approaches permit this. A companion effort is addressing design of anode sleds per se. Relatedly, progress has also been in adapting the recently developed Slope Parameter cp design method to pipelines, although this is likely to be of use more in cp design for new rather than for retrofit installations. In the remainder of the project, efforts will be focused upon continued development of the first-principles based equation and its application to design and to development of a simplified retrofit design format spreadsheet.

TABLE OF CONTENTS

INTRODUCTION

General

While pipelines are generally recognized as the safest means of transportation for oil and gas offshore, still failures occur because of 1) material and equipment problems, 2) operational errors, 3) corrosion, 4) storms/mud slides, and 5) third party incidents (mechanical damage). These, in turn, can result in pollution, loss of product availability, repair expenses, business interruption, and litigation. Several reports and publications are available that evaluate the occurrence and cause of offshore Gulf of Mexico pipeline failures (1-3). These indicate that 690 pipeline accidents of sufficient magnitude to be recorded by the MMS occurred during the twenty year period from 1967 to 1987. Of these, 343 (50 percent) resulted from corrosion with a total of 85 percent of these being documented as involving either external or general attack. During this same period the failure rate increased at an average of over two per year. This trend is thought to have been a consequence of 1) increased pipeline population and offshore construction activity with time and 2) aging of the pipeline infrastructure. At the same time, relatively little attention has been directed toward this particular problem (external corrosion of marine oil and gas pipelines), as evidenced by the fact that the 1991 International Workshop on Offshore Pipeline Safety (4) included only one paper which explicitly focused upon this topic.

Structural and high strength steels have historically been the only economically viable material for construction of marine petroleum transport pipelines. However, the inherent lack of corrosion resistance of this material class in sea water and the consequences of pipeline failure require that corrosion control systems be designed, installed, and maintained such that a high degree of reliability is realized. Reliability considerations have become magnified in recent years with the transition from relatively shallow to deepwater installations. While cathodic protection (cp) has historically been employed as the sole corrosion control methodology for the submerged portion of petroleum production platforms, both mobile and fixed, the one-dimensional nature of pipelines is such that the combined use of coatings with cp is required. In the former case (platforms), anode resistance and current density demand are the fundamental parameters that are important in cp design. For pipelines, however, coating quality and metallic path resistance must also be taken into account, at least in the generalized case. Pipeline cp systems can be of either the impressed current or galvanic type; however, applicability of the former is normally limited to 1) proximity of landfall whereby protection is provided seaward by a shore-based rectifier and anode bed to a distance that is defined by the "throwing power" of the system and 2) a pipeline run between two platforms where the pipe length is sufficiently short that the entire line can be protected by a single rectifier and anode or anode template at one or both ends. In each case, the limiting distance to which protection is affected is defined by the voltage drop along the metallic pipeline that arises in conjunction with the current

return to ground. The higher the coating quality, the less the pipe current demand and the greater the distance to which protection is extended. However, coating quality of marine pipelines has invariably been below that of buried onshore counterparts so that this distance is considerably less in the former case than the latter. Also, achievement of adequate protection at a distant point likely involves overprotection in the vicinity of the rectifier. Such overprotection can cause coating damage with time, in which case the pipe current demand increases and the distance to which protection is extended becomes less. Because of these factors, corrosion control for the great majority of marine pipelines is provided by galvanic anodes of the bracelet type, as illustrated schematically in Figure 1. Because of restrictions upon the size of bracelet anodes that arise from structural and installation considerations, the spacing between these is normally limited to a maximum of 100-200 meters. Consequently, voltage drop in the pipeline is insignificant; and system life is governed by anode mass considerations.

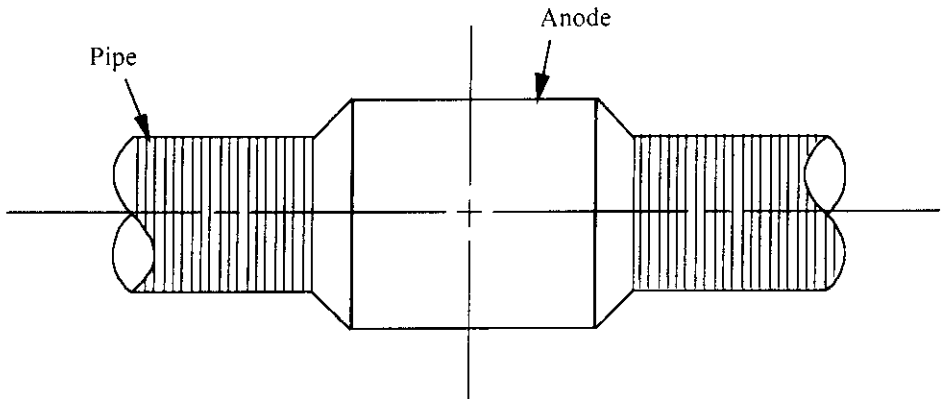

Figure 1: Schematic illustration of an offshore pipeline galvanic anode.

It is generally recognized that corrosion of steel in sea water is arrested by polarization to a potential of $-0.80\ V_{AgCl}$ or more negative, and so achieving and maintaining this potential has been established as the goal of cathodic protection (5,6). Figure 2 illustrates schematically a pipeline with identical, equally spaced anodes and the resultant potential profile. Thus, the pipeline is most polarized immediate to the anodes; and potential attenuates with increasing distance therefrom. Portions of the pipeline for which potential is $-0.80\ V_{AgCl}$ or more negative are protected and unprotected where potential is more positive.

The equations of Morgan (7) and Uhlig (8) have been employed historically to project 1) potential attenuation along a pipeline and 2) the current requirement to achieve that profile in terms of coating and pipe properties and pipe dimensions. Thus, from the cp current components and resultant potentials illustrated in Figure 3, Morgan established a differential equation the solution of which is

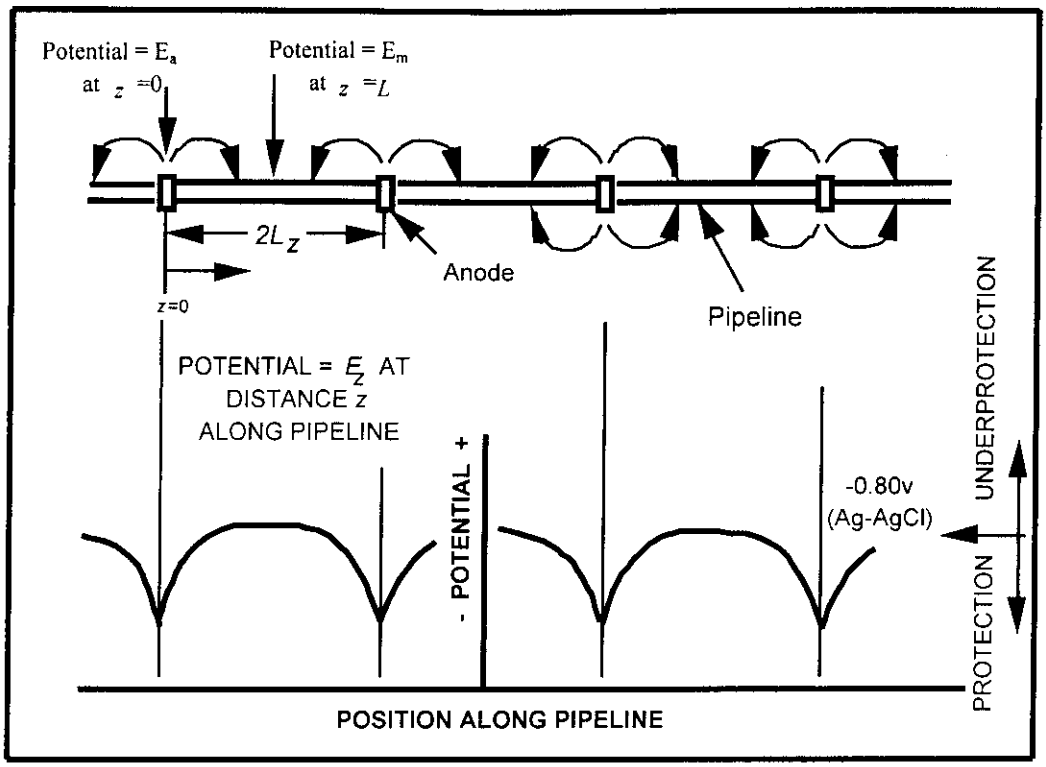

Figure 2: Schematic illustration of a cathodically polarized pipeline and the resultant potential profile.

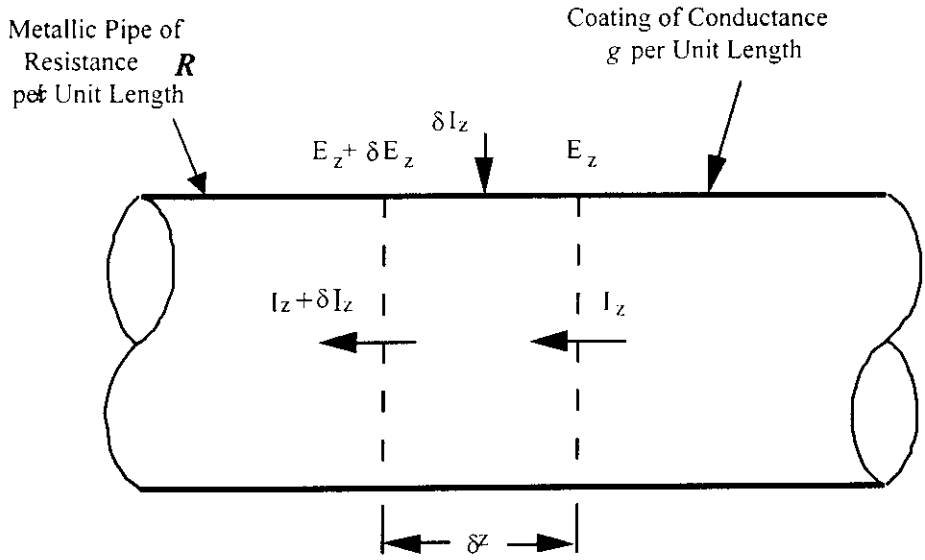

Figure 3: Current and potential in a cathodically polarized pipe element.

$$E_z = E_m \cdot \cosh \alpha' (L - z)$$
$$E_a = E_m \cdot \cosh(\alpha' \cdot L) \qquad (1$$

where E_z and E_m are defined in Figure 2 and α', the attenuation constant, equals $\sqrt{R/\zeta}$ or the ratio of the

square root of the metallic pipeline to coating resistance per unit length. Further, on the basis that the design for an existing pipeline is adequate such that protection is achieved and that sufficient anode mass remains, the corresponding anode current output is

$$I_a = 2\left(\frac{2}{r_p}\right)\alpha' \cdot E_m \cdot \sinh\left(\alpha' L\right), \qquad (2$$

where r_p is the pipe radius. On the basis of these assumptions, the current projected by this relationship constitutes the pipe current demand.

As a refinement to the pipeline potential attenuation equation of Morgan, Uhlig (8) proposed the relationships

$$E_z = E_m \cdot \cosh\left[\left(\frac{2\pi r_a \cdot R_m}{k \cdot \zeta}\right)^{1/2} \cdot (z - L)\right] \text{ and}$$

$$E_a = E_m \cdot \cosh\left[-\left(\frac{2\pi r_a \cdot R_m}{k \cdot \zeta}\right)^{1/2} \cdot L\right], \qquad (3$$

where k is a constant that reflects 1) polarization characteristics of bare metal exposed at the base of coating defects and 2) effective coating resistivity. Correspondingly, Uhlig's equation for anode current output is

$$I_z = \left(\frac{2E_B}{R_m}\right) \cdot \left(\frac{2\pi r_a \cdot R_m}{k \cdot \zeta}\right)^{1/2} \cdot \sinh\left[\frac{z}{2} \cdot \left(\frac{2\pi r_a \cdot R_m}{k \cdot \zeta}\right)^{1/2}\right]. \qquad (4$$

If, in addition to sufficient anode mass being present, the coating quality is good, then Equations 1 and 3 project potential attenuation to $z = L$ (the one-half anode spacing position or location where potential should be most positive) to be minimal (perhaps a few millivolts or less) provided anode spacing is not excessive. However, this attenuation should increase with time as anodes expire (current output per anode decreases) or the coating deteriorates (or both); and eventually the current demand of the pipeline exceeds the anode output capability. The onset of such potential attenuation is a fundamental indicator that the need for cp retrofit is eminent even though the pipeline may still be protected (E_z more negative than -0.80 V_{AgCl} everywhere along the line). However, the time frame during which this transition from protection to under-protection transpires may be relatively short compared to that for a jacket type structure, as addressed subsequently. A fundamental limitation of Equations 1-4 is that they consider only the coating and

pipeline, but not anode, resistance terms. Consequently, this approach precludes 1) optimization of anode spacing and 2) evaluation of anode expiration and the onset of under-protection. Also, the potential profile that is projected may by non-conservative (less protective) than is actually the case.

More recently, Boundary Element Modeling (BEM) has been applied to analysis of potential attenuation along pipelines and anode current output. This approach utilizes a numerical algorithm for the solution of a Laplace type governing equation,

$$\nabla^2\phi = \frac{\partial^2\phi}{\partial x^2} + \frac{\partial^2\phi}{\partial y^2} + \frac{\partial^2\phi}{\partial z^2} = 0\,, \qquad (5$$

that describes the potential variation in an electrolyte. To model an electrochemical process, the Laplace equation is used in conjunction with specified boundary conditions that portray the geometry and effects of electrical sources and sinks. However, while this approach incorporates the electrolyte and coating resistance terms, it excludes the metallic pipe path component. Consequently, it can provide no quantitative information relevant to optimization of anode or anode ground bed spacing.

Present Design Protocol for Cathodic Protection of Offshore Platforms

Cathodic protection design procedures have evolved historically according to:

1. Trial and error.
2. Ohm's law employing a single, long-term current density (9).
3. Ohm's law and rapid polarization employing three design current densities, an initial (i_o), mean, (i_m), and final (i_f) (5,6).
4. The slope parameter method (10-13).

Accordingly, practices 2) and 3) are based upon the equation

$$I_a = \frac{\phi_c - \phi_a}{R_a}\,, \qquad (6$$

where

I_a = individual anode current output,

ϕ_c = closed circuit cathode potential,

ϕ_a = closed circuit anode potential, and

R_a = resistance of an individual anode.

As noted above, anode resistance is normally the dominant component of the total circuit resistance for space-frame structures such as platforms, and so it alone need be considered here. In most cases, this parameter is calculated from standard, numerical relationships that are available in the literature (14-19) based upon anode dimensions and electrolyte resistivity. Figure 4 graphically illustrates the principle behind this equation and approach.

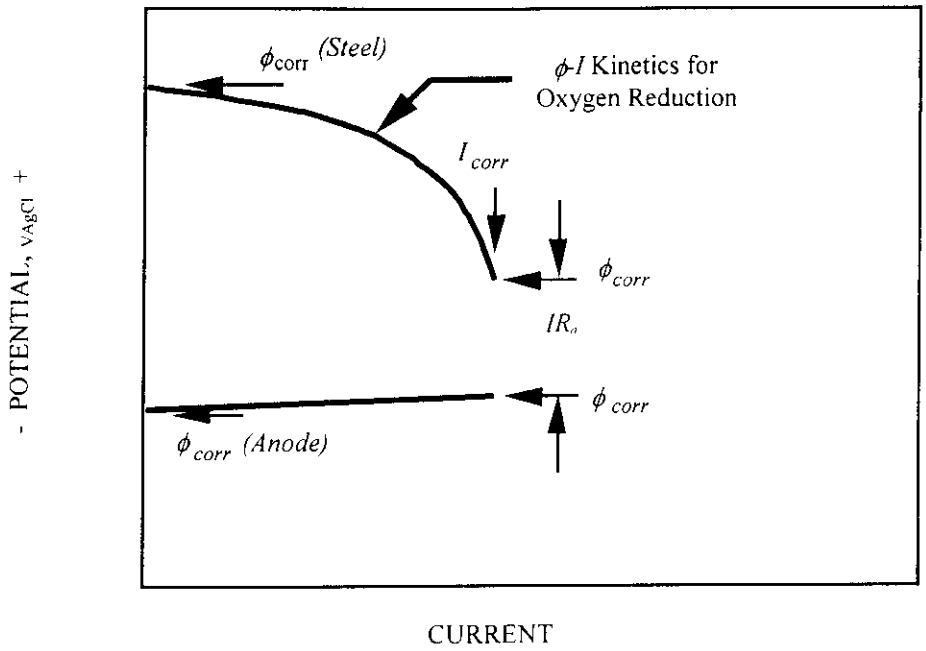

Figure 4: Schematic illustration of a polarization diagram and of parameters relevant to galvanic anode cathodic protection system design.

Considering that the net current for protection, I, is the product of the structure current density demand (i_c) and surface area (A_c), the number of anodes required for protection, N, is determined from the relationship

$$N = \frac{i_c \cdot A_c}{I_a}. \qquad (7$$

By earlier practice (9), cp design was based upon a single, time average or mean current density that polarized the structure to the potential required for protection (-0.80 V_{AgCl}) within perhaps several months to one year. It was subsequently recognized, however, that application of an initially high current density (rapid polarization (20-25)) resulted in a lower mean current density and reduced anode mass to provide protection for the design life. Accordingly, present protocols (5,6) are based upon three current densities,

an initial (i_o), mean (i_m), and final (i_f), where the first is relatively high and is realized upon initial deployment, the second is the time-averaged value, and the last reflects what is required near the end of the design life. Values for i_o and i_f are determined by substituting each of these parameters for i_c in Equations 5 and 6 with the number of anodes being determined therefrom. On the other hand, i_m is calculated from the mass balance relationship

$$N = \frac{i_m \cdot A_c \cdot T}{C \cdot w}, \qquad (8$$

where

T = design life of the cp suystem,
C = anode current capacity, and
w = weight of an individual anode.

Invariably, the number of anodes determined according to each of the three calculations is different with the largest being specified. For uncoated structures this is usually i_o. Consequently, the system is over-designed in terms of the other two current densities. This arises because the procedure is an algorithm rather than being first principles based.

More recently, the slope parameter approach (10-13) to galvanic cp system design was developed based upon a modification of Equation 6 as

$$\phi_c = \left(R_t \cdot A_c\right) \cdot i_c + \phi_a, \qquad (9$$

where R_t is the total circuit resistance. This relationship projects a linear interdependence between ϕ_c and i_c provided R_t, A_c, and ϕ_a are constant. That this is normally the case has been confirmed by both laboratory and field measurements (10-13). For space frame type structures with multiple galvanic anodes,

$$R_t \cong \frac{R_a}{N}; \qquad (10$$

with the product $R_t \cdot A_c$ being defined as the slope parameter, S, such that

$$S = \frac{R_a \cdot A_c}{N}. \qquad (11$$

Substitution of the latter expression into Equation 8 then yields

$$R_a \cdot w = \frac{i_m \cdot T \cdot S}{C}. \qquad (12$$

Upon defining an appropriate value for S, all terms on the right side are known from the design choices; and so the process is reduced to determination of the optimum combination of R_a and w. This may be accomplished in terms of anodes of standard dimensions or, perhaps more effectively, by specifying an elongated anode or dualnodes (26). Thus, if anode resistance is represented in terms of Dwight's modified equation,

$$R_a = \frac{\rho}{2\pi L} \cdot \left[\ln\left(\frac{4l}{r}\right) - 1 \right], \qquad (13$$

where

ρ = electrolyte resistivity,
l = anode length, and
r = equivalent anode radius,

then the left side of Equation 12 becomes

$$R_a \cdot w = \frac{\rho \cdot \rho' \cdot r^2 \cdot v}{2} \left[\ln \frac{4L}{r} - 1 \right], \qquad (14$$

where

ρ' = anode density and
v = volume fraction of the anode that is galvanic metal as opposed to core.

The required number of anodes can then be calculated from Equation 11.

Hartt et al. (11) projected that the slope parameter based design approach yields a 32 percent reduction in anode mass in the case of typically sized structures compared to design according to present recommended practice (5,6). This arises because Equation 14 is first principles based and incorporates both i_m and i_o, the former explicitly and the latter implicitly via the slope parameter. As such, design can be

optimized in terms of both parameters instead of just one. An alternative view is that, of the two terms on the left side of Equation 14, R_a determines i_o while w relates to i_m.

Present Design Protocol for Cathodic Protection of Marine Pipelines

Two fundamental differences between offshore platforms and pipelines are, first, the three dimensional nature of the former compared to one dimensional for the latter and, second, the fact that pipelines are invariably coated while platforms are normally not. Because of the second consideration, design of the cp system for pipelines precludes i_o; and i_m alone or perhaps i_f also need be taken into account Thus, marine pipeline cp design (5,6) considers the current demand, I_c, as

$$I_c = A_c \cdot f_c \cdot i_c, \qquad (15$$

where i_c is normally in the range 60-170 mA/m^2 depending upon pipe depth, temperature, sea water versus mud exposure, and whether or not the calculation is for the mean ($I_c = I_m$)or final ($I_c = I_f$) condition, where I_m is the time-averaged net current and I_f is the net current near the end of the design life. Correspondingly, the net anode mass, M, is determined from a modified form of Faraday's law,

$$M = \frac{8{,}760 \cdot I_m \cdot T}{u \cdot C}, \qquad (16$$

where u is a utilization factor; and current output of individual anodes is calculated from Equation 6. The number of bracelet anodes that are spaced equally alone the pipeline is then determined as

$$N = \frac{I_c}{I_a}. \qquad (17$$

A shortfall of the above analysis is it assumes that the spacing between anodes is limited such that metallic path resistance is negligible. Consequently, this method is not applicable to designs that call for maximizing anode or anode sled spacing, as is likely to be critical in the case of retrofits.

PROJECT OBJECTIVES

Oil and gas transportation pipelines have now been in service in shallow Gulf of Mexico waters for as

long as about five decades. During this time, the technology for protecting these from external corrosion has evolved such that it is now recognized that the cp criteria and approaches used for earlier generation lines may not have been adequately conservative. Specific examples of this include the following:

1. The spacing of galvanic anodes on early generation pipelines was typically one-quarter mile (400 m). However, present designs involve spacings as short as 120 m to account for the possibility of electrical connection damage during the laying operation such that some anodes are lost or do not properly activate.

2. Pipeline laying technology has improved with time such that damage to anodes upon installation is less likely.

3. Performance is generally better for anodes produced today compared to those of several decades ago.

Additional concerns are, first, the life of older pipelines has often been extended beyond that for which the cp system was originally designed; second, pipeline corrosion inspections are often neither sufficiently sensitive or sufficiently comprehensive to necessarily disclose problems; and, third, pipelines may experience modified service conditions. The present project was initiated in 1997 with the objective of defining criteria and a standardized practice for retrofitting the cathodic protection system on older marine pipelines. This report describes progress that has been made to-date. Activities have involved, first, modification of the Slope Parameter cp design method to pipelines and, second, development of a first principles based equation for potential attenuation alone a pipeline and anode current output. These, along with the implications of each are described below.

PROPOSED SLOPE PARAMETER DESIGN METHOD

Application of Equation 9 to a coated, cathodically polarized pipeline requires that 1) spacing between anodes be sufficiently small that metallic path resistance is negligible, 2) pipe resistance to sea water is negligible, 3) all current enters the pipe at holidays in the coating (bare areas), and 4) ϕ_c and ϕ_a are constant with both time and position. As a consequence of 1) and 2), $R_t \cong R_a$; and from 3),

$$A_{c(1)} = \frac{2\pi \cdot r_p \cdot L_{as}}{\gamma}, \qquad (18$$

where $A_{c(1)}$ is the pipe surface area protected by a single anode, γ is the ratio of total pipe surface area to bare surface area (this parameter is a modification of the coating breakdown factor, f_c, that was introduced in conjunction with Equation 15), and L_{as} is the anode spacing or $2L$. Table 1 provides a comparison between γ and the coating breakdown factor, f_c. Combining Equations 9 and 18 and solving for L_{as} then yields

Table 1: Correspondence of the Coating Breakdown Factor and γ to the percentage of bare area and the corresponding $\alpha \cdot \gamma$ for α values of 20, 40, and 60 $\Omega \cdot m^2$.

BARE AREA, %	COATING BREAKDOWN FACTOR	γ	ASSUMED α, $\Omega.m^2$	CORRESPONDING $\alpha\gamma$, Ωm^2
0	0	∞	-	-
2	0.02	50	20	1,000
			40	2,000
			60	3,000
5	0.05	20	20	400
			40	800
10	0.1	10	60	1,200
			20	200
			40	400
			60	600
100	1	1	20	20
			40	40
			60	60

$$L_{as} = \frac{(\phi_c - \phi_a) \cdot \gamma}{2\pi \cdot r_p \cdot R_a \cdot i_c}. \qquad (19$$

Assuming that ϕ_c and i_c exhibit a linear interdependence, then

$$i_c = \frac{\phi_{corr} - \phi_c}{\alpha}, \qquad (20$$

where ϕ_{corr} is the free corrosion potential and α is the polarization resistance. Combining Equations 19 and 20 leads to an initial design expression for anode spacing as

$$L_{as} = \frac{(\phi_c - \phi_a)}{\phi_{corr} - \phi_c} \cdot \frac{\alpha \cdot \gamma}{2\pi \cdot r_p \cdot R_a}; \qquad (21$$

or, alternatively,

$$\phi_c = \frac{\phi_{corr} + (\phi_a \cdot \psi)}{1 + \psi}, \qquad (22$$

where

$$\psi = \frac{\alpha \cdot \gamma}{2\pi \cdot r_p \cdot L_{as} \cdot R_a}.$$

The corresponding design life can be calculated from the modified version of Equation 8,

$$T = \frac{w \cdot C \cdot u}{i_m \cdot A_{c(1)}}. \qquad (23$$

Finally, upon combining Equations 18, 20, and 23,

$$T = \frac{w \cdot C \cdot u \cdot \alpha \cdot \gamma}{\left(\phi_{corr} - \phi_c\right) \cdot 2\pi \cdot r_p \cdot L_{as}}. \qquad (24$$

Since the term $2\pi \cdot r_p \cdot L_{as} \cdot R_a / \gamma$ (Equation 24) is equivalent to S (Equation 9), this approach is termed the Slope Parameter method for pipeline cp design. However, the magnitude of this slope parameter differs from that of bare steel (10-13) by a factor of $1/\gamma$. On the basis that an upper limit of i_m for most pipeline cp designs is 75 mA/m^2 (at ϕ_c = -0.80 $V_{Ag/AgCl}$), then $\alpha \geq 2.0\ \Omega \cdot m^2$. Considering further a realistic upper limit for the coating breakdown factor as seven percent (γ = 14.3) leads to the likely range for $\alpha \cdot \gamma$ being equal or greater than 30 $\Omega \cdot m^2$.

The initial step for a given design then is to calculate a baseline L_{as} in terms of $\alpha\gamma$, R_a (actually, anode surface area or dimensions using, for example, McCoy's formula (27), and ϕ_c (design cathode potential) using Equation 21. Upon substitution of this L_{as} into Equation 15 and possibly with iteration via Equation 24 (such iteration may be necessary since anode dimensions and w are interrelated and changes in these, in addition to changes in L_{as} and $\alpha\gamma$, result in a different ϕ_c and T, as calculated by Equation 24), w and T are optimized.

Consider as an example the pipeline and cp design choices listed in Table 2. For these, and assuming 1) a standard 60.8 kg bracelet anode of length 0.432 m and outer radius 0.187 m, ϕ_c = -0.975 $V_{Ag/AgCl}$ (this constitutes a design polarized potential), and 3) R_a = 0.353 Ω as determined from McCoy's formula (27),

$$R_a = \frac{0.315 \cdot \rho_e}{\sqrt{A}}, \qquad (25$$

where A is the anode surface area, then Equation 21 indicates L_{as} = 170 m. From Equation 24, the corresponding life is 30.1 years, which is consistent with the design requirement (Table 2). If these values differ significantly, then iteration between Equations 22 and 24 based upon alternative choices for w (or R_a), α, γ, or L_{as} (or for a combination of two or more of these terms) is required.

Table 2: Listing of pipe and electrolyte properties and design choices used in the example.

Pipeline Outer Radius, m	0.136
Pipeline Inner Radius, m	0.128
Electrolyte Resistivity, $\Omega \cdot m$	0.80
Alpha, $\Omega \cdot m^2$	7.5
Gamma	20
Design Life, years	30
Anode Current Capacity, Ah/kg	1,700
Anode Utilization Factor	0.8
Open Circuit Anode Potential, $V_{Ag/AgCl}$	-1.05

This proposed method is considered to be an improvement upon the existing pipeline cp design approach because of the additional parameters that it incorporates, and its accuracy is quantified in comparison to the first principles based attenuation equation that is presented subsequently in a later section. As an added consideration, a fundamental parameter that is critical to any cp design, either for a new structure or as a retrofit, is current density demand; that is, the magnitude of current that anodes must provide to achieve protection. At the same time, determination of current demand is difficult; and so this parameter is normally assigned a value that is considered to be sufficiently high that corrosion protection results. Such an approach results in over-design, however, by an undisclosed amount. Equation 21 provides an alternative to this the case of existing pipelines in that the $\alpha\gamma$ term constitutes current density demand and all other terms are known, either from construction records or from pipeline survey records. A limitation, however, is that Equation 21 assumes, first, that the pipeline remains polarized and, second, metallic path resistance is negligible; and so an alternative method must be devised for these situations Consequently, Equations 21 and 24 cannot be used in their present form to project a maximum allowable anode sled spacing, as is critical to retrofit cp design.

PROPOSED INCLUSIVE POTENTIAL ATTENUATION AND ANODE CURRENT OUTPUT EQUATION

The Governing Equation

A first principles based equation has been derived that includes all three resistance terms (electrolyte, coating, and metallic path), in addition to polarization resistance. Details of the derivation have been reported elsewhere (28) and are not repeated here. The approach considers that electrode (pipe) potential, $\phi_c(z)$, could be represented as the charge gradient associated with the double layer or

$$\phi_c(z) = U_m(z) - U_e(z) + K_{ref}\,, \tag{26}$$

where $U_m(z)$ and $U_e(z)$ are the metallic and electrolyte potentials, respectively, and K_{ref} accounts for the fact that $\phi_c(z)$ must be measured relative to a reference potential (constant). Also,

$$E_c(z) = \phi_c(z) - \phi_{corr}\,, \tag{27}$$

where $E_c(z)$ is the magnitude of polarization. Further, upon taking the second derivative of Equations 26 and 27 and combining,

$$\frac{\partial^2 E_c}{\partial z^2} = \frac{\partial^2 U_m}{\partial z^2} - \frac{\partial^2 U_e}{\partial z^2}\,. \tag{28}$$

Development of expressions for each of the three component terms, E_c, U_m, and U_e, and substitution of these into Equation 28 led to the governing equation

$$\frac{\partial^2 E_c(z)}{\partial z^2} + \frac{\partial E_c(z)}{\partial z}\cdot H\cdot\left(\frac{1}{r_a} - \frac{1}{z}\right) + E_c(z)\cdot\left(\frac{2H}{z^2} - B\right) = 2H\cdot\frac{1}{z^3}\cdot\int_z^L E_c\left(z^*\right)dz^*\,, \tag{29}$$

where r_a is the radius of identical spherical anode superimposed upon the pipe at intervals of $2L$ and

$$H = \frac{\rho_e \cdot r_p}{\alpha\gamma} \text{ and}$$

$$B = \frac{R_m \cdot 2\pi r_p}{\alpha\gamma}\,,$$

where ρ_e is electrolyte resistivity, A linear relationship was assumed between ϕ_c and i_c such that α may be visualized, as shown in Figure 5. Because there is no known solution to Equation 29, it must be solved numerically. This was done using a Finite Difference Method (FDM).

Verification and Comparison of Approaches

Figure 6 presents a plot of pipe potential as a function of distance from an anode as determined by 1) Equation 3, 2) Boundary Element Modeling (BEM), and 3) a Finite Difference Method (FDM) solution of

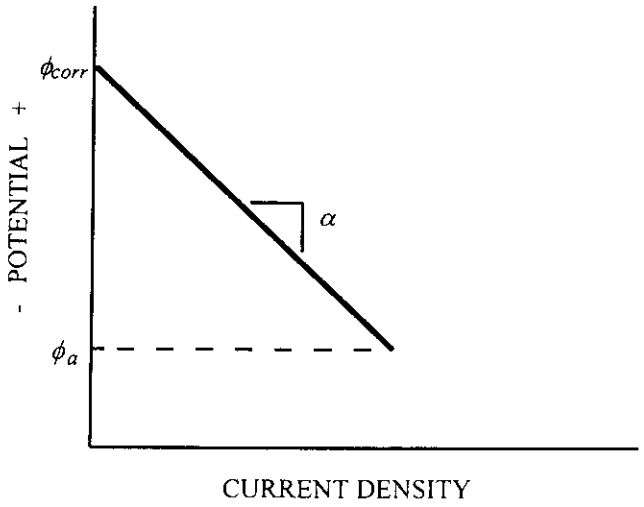

Figure 5: Proposed ϕ_c versus i_c relationship with definition of α.

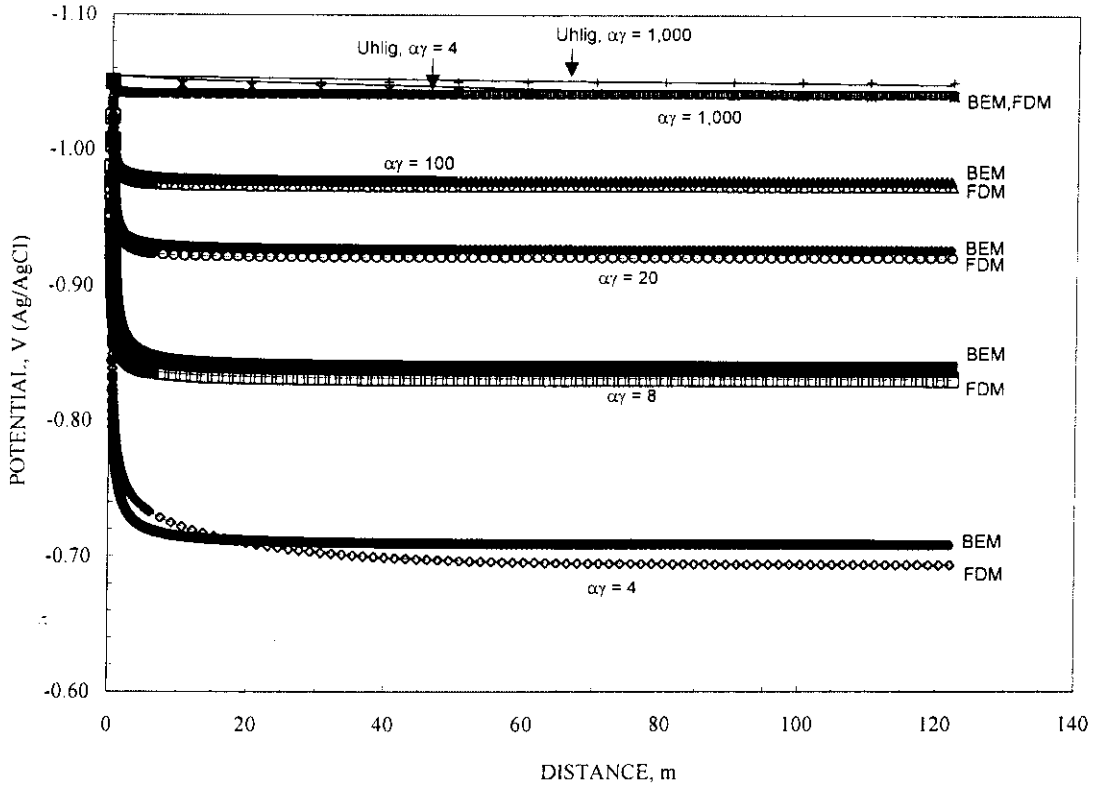

Figure 6: Potential as a function of distance for a pipeline protected by identical anodes spaced 244 m apart and with $\alpha \cdot \gamma$ values of 4, 8, 20, and 100 $\Omega \cdot m^2$.

Equation 29 for $\alpha \cdot \gamma$ values of 4, 20, 100, and 1,000 $\Omega \cdot m^2$ (an $\alpha \cdot \gamma$ of 4 $\Omega \cdot m^2$ corresponds to a bare pipe with a current density demand of 100 mA/m^2 at –1.05 $V_{Ag/AgCl}$, whereas an $\alpha \cdot \gamma$ of 1,000 $\Omega \cdot m^2$ corresponds, for example, to four percent bare area (γ = 25) and α = 40 $\Omega \cdot m^2$ (current density demand of 10 mA/m^2 at –1.05 $V_{Ag/AgCl}$)). As such, these represent realistic extremes of conditions that are likely to be encountered in practice. Other pipe and electrolyte parameters are as listed in Table 3. For these conditions, the solutions to Equation 3 are relatively insensitive to coating quality and current density demand ($\alpha \cdot \gamma$) and are non-conservative compared to the BEM and Equation 29 results in that they predict greater cathodic polarization. The Equation 29 and BEM potential profiles, on the other hand, are in good mutual agreement. These are characterized by a potential decay within approximately the first 10 m of the anode, the magnitude of which is determined by 1) anode resistance (dimensions and electrolyte resistivity) and 2) the pipe current demand ($\alpha \cdot \gamma$). For each specific case, potential is relatively constant and is defined by the voltage drop associated with the anode. The finding that the FDM plateau potential is slightly more negative than the BEM one and that the magnitude of this difference is inversely related to $\alpha \cdot \gamma$ is probably due to inclusion of the metallic path resistance term in the former solution and its exclusion in the latter. However, the difference in the two plateau potentials is not considered to be of practical significance. Because of the close correspondence between the BEM and FDM results and because BEM is a proven methodology for quantitatively characterizing potential fields, it is concluded that the FDM solution to Equation 29 is an appropriate means for projecting potential attenuation along pipelines and anode current output.

Table 3: Pipe and electrolyte parameters for the analyses shown in Figure 6.

Pipeline Outer Radius, m	0.136
Pipeline Inner Radius, m	0.128
Anode Spacing, $2L$, m	244
Equivalent Sphere radius of Anode, m	0.201
Electrolyte Resistivity, Ω·m	0.30
Pipe Resistivity, Ω·m	17×10^{-8}
Free Corrosion Pipe Potential, $V_{Ag/AgCl}$	-0.65
Anode Potential, $V_{Ag/AgCl}$	-1.05

As a further confirmation, Figure 7 presents attenuation profiles from 1) BEM, 2) the FDM solution to Equation 29 with $\rho_m = 17 \cdot 10^{-8} \Omega \cdot m$ (the same as in Figure 6), and 3) the FDM solution to Equation 29 with ρ_m = 0 for the same anode and pipe dimensions as for Figure 6 ($\alpha\gamma$ = 100 $\Omega \cdot m^2$, and L = 3,000 m). The ϕ_c versus z trend is characterized in each of the three cases by the same, relatively abrupt potential increase in the immediate vicinity of the anode that was apparent in Figure 6; but the FDM solution that

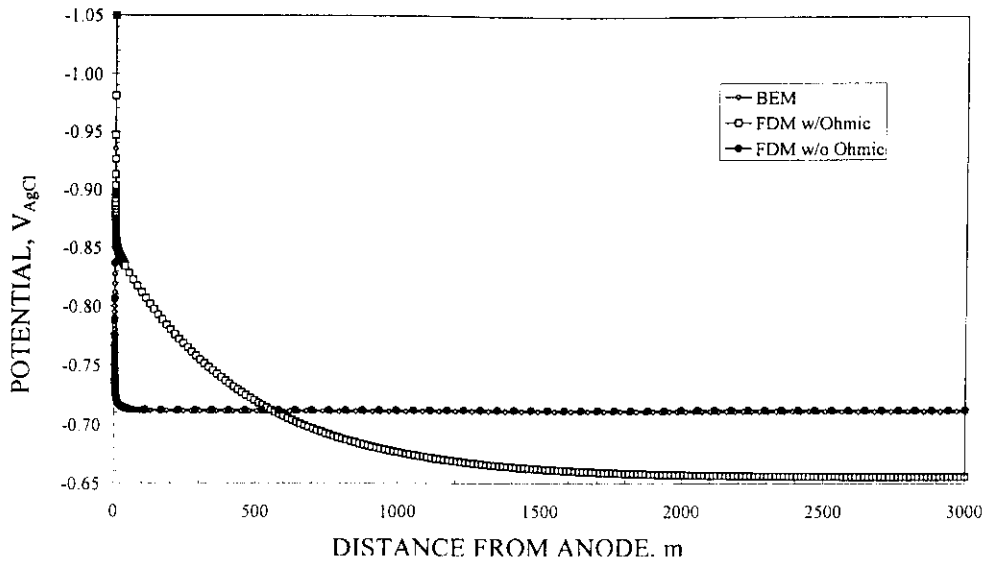

Figure 7: Comparison of BEM and FDM solutions to Equation 29 where the latter reflect presence and absence of the metallic path resistance term.

includes the metallic path resistance term exhibits a further attenuation, albeit of a lesser magnitude, along the entire range of z, whereas the BEM and FDM solution that does not consider metallic path resistance essentially superimpose with little additional attenuation beyond the vicinity of the anode. Thus, while the BEM and FDM (metallic path resistance term included) solutions are essentially the same for relatively small L, the latter projects increasing attenuation compared to the former with increasing anode spacing. On the other hand, it can be shown that Equation 29 reduces to the Uhlig expresion for R_a = 0. Consequently, potential attenuation projected by BEM is non-conservative for situations where metallic path resistance is not negligible; and the Uhlig equation is non conservative in cases where anode resistance is not negligible. It is concluded that Equation 29 provides a means for accurately assessing potential attenuation along a cathodically polarized pipeline and is likely to be the most accurate method for situations where both $E_e(z)$ and $E_m(z)$ are not negligible. The research effort is now focusing upon strategies whereby Equation 29 can be integrated into retrofit pipeline cp design protocols.

Anode current output can be determined from both BEM and the FDM solution of Equation 29, since $E_e(z)$ is proportional to current demand which, in turn, dictates I_a. Thus, Figure 8 presents a plot of I_a versus $\alpha\gamma$ as determined by BEM, the FDM solution to Equation 29, and Uhlig (Equation 3) based upon the same pipe and electrolyte parameters that were employed in conjunction with Figures 6 and 7. This reveals that results from the former two methods (BEM and FDM) are in excellent mutual agreement, whereas Uhlig's equation overestimated I_a in the lower $\alpha\gamma$ range, presumably because of failure of this expression to adequately address the near-field and the greater influence of the near-field at relatively low $\alpha\gamma$. The Uhlig expression projects I_a with reasonable accuracy in cases where current demand and coating quality are such

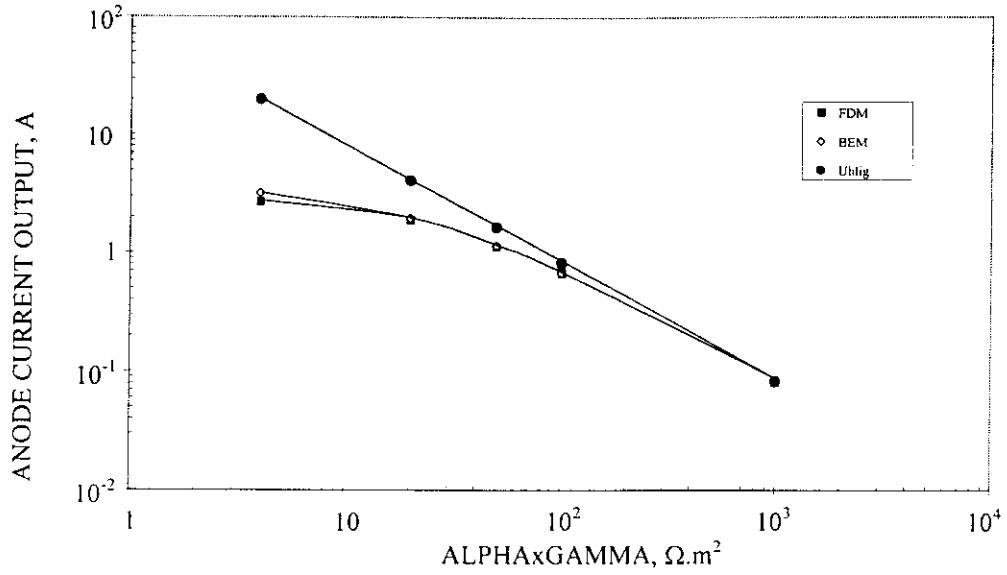

Figure 8: Comparison of anode current output as projected by BEM, FDM, and Equation 3.

that $\alpha\gamma \geq 100\ \Omega \cdot m^2$. However, the BEM method is expected to overestimate I_a also for $2L$ values for which metallic resistance is no longer negligible.

The results in Figures 6 and 7 indicate that a FDM solution to Equation 29 provides an accurate projection of potential attenuation along a pipeline or riser and of anode current output. Because the equation incorporates the electrolyte, coating, and metallic resistance terms, it represents an improvement over the Uhlig expression except in situations where electrolyte resistance is negligible and over BEM where metallic path resistance is non-negligible. On this basis, Equation 29 has utility for design of both new and retrofit cathodic protection systems.

Effect of Anode Spacing and Pipe Current Density Demand upon Potential Attenuation and Current Output

Figures 9 and 10 present attenuation profiles for different pipeline lengths from 200 to 3,000 m and $\alpha \cdot \gamma$ =100 Ω·m^2 in the former case and for anode spacings from 100 to 10,000 m and $\alpha \cdot \gamma$ = 1,000 Ω·m^2 in the latter. The same pipe and environment parameters in Table 3 apply here as well. These plots indicate that the difference between the two analysis methods (BEM and Equation 29) increases with 1) increasing distance from an anode, 2) increasing anode spacing, and 3) decreasing $\alpha \cdot \gamma$. The FDM solution is considered to be the more accurate of the two methods, at least for situations where metallic path resistance is non-negligible. On this basis, situations can arise where BEM indicates protection along the entirety of a pipeline but, in fact, under-protection exists beyond a certain distance. Accordingly, Equation 29 is recommended as the analysis method of choice.

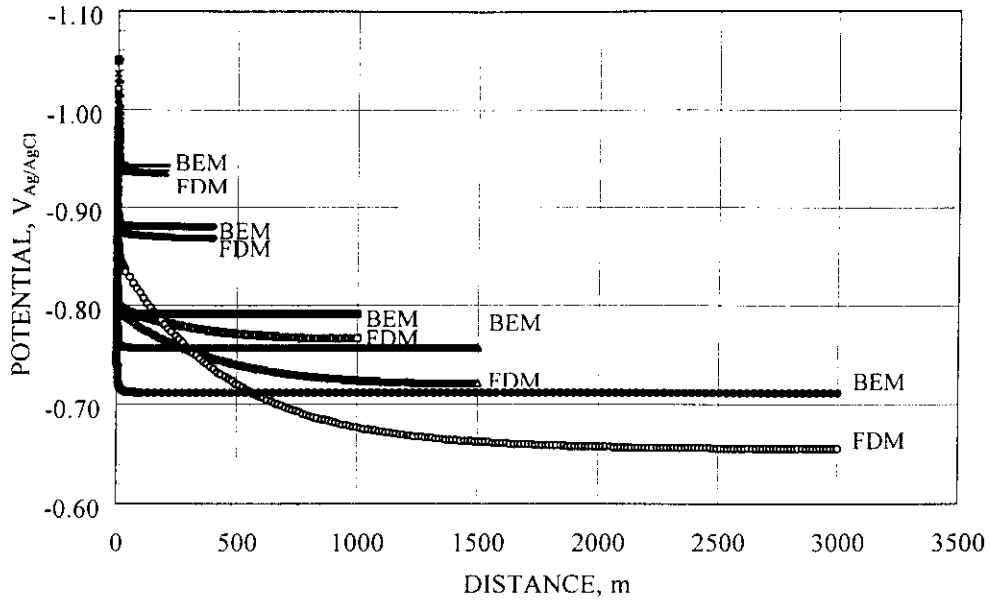

Figure 9: Comparison of BEM and FDM potential profiles for pipelines with anode spacings from 200 to 3,000 m and with $\alpha \cdot \gamma = 100\Omega \cdot m^2$.

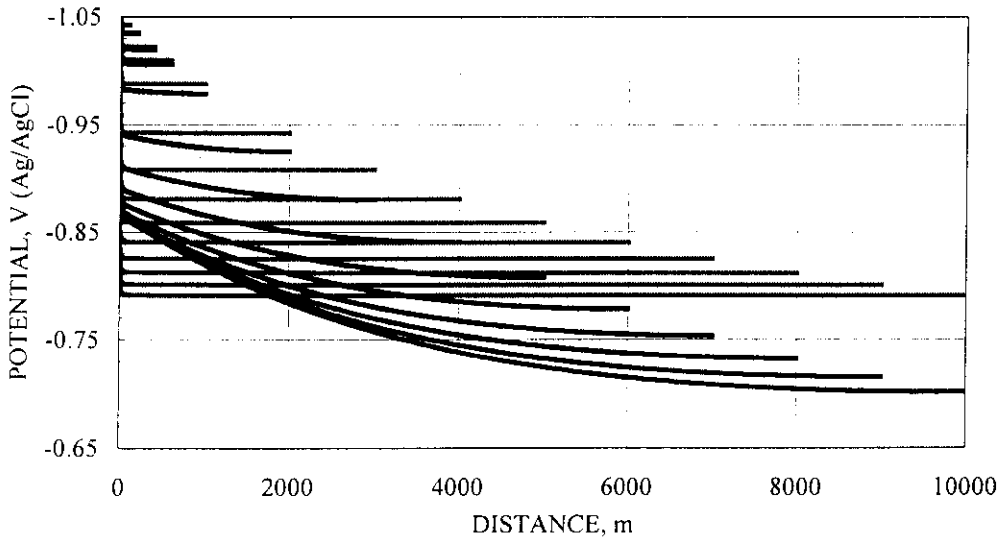

Figure 10: Comparison of BEM and FDM potential profiles for pipelines with anode spacings from 100 to 10,000 m and with $\alpha \cdot \gamma = 1{,}000\Omega \cdot m^2$. The more negative profile for each pipe length is the BEM solution and the more positive the FDM.

Figures 11 and 12 show plots of anode current output as a function of half anode spacing for the same situations depicted in Figures 9 and 10, respectively. The BEM and FDM solutions are in good agreement for relatively short spacings, but for greater ones the former projects that this current increases progressively with increasing anode spacing whereas the FDM shows a maximum beyond which current decreases. The latter effect is more pronounced in the lower $\alpha \cdot \gamma$ case. Again, this difference is apparently due to BEM not including the metallic path resistance term. Also, the situations in Figures 9

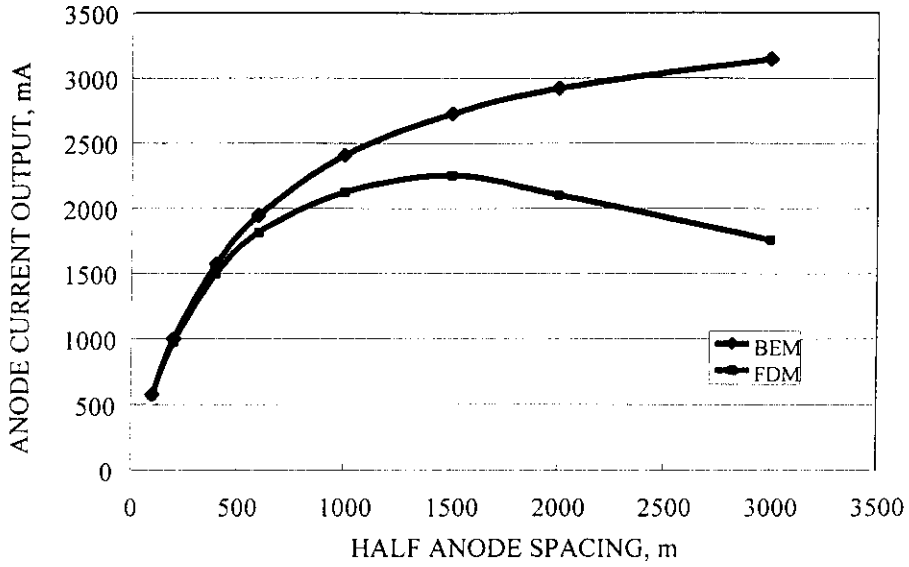

Figure 11: Anode current output, as projected by BEM and Equation 29 (FDM) as a function of half anode spacing and for $\alpha \cdot \gamma = 100\Omega \cdot m^2$.

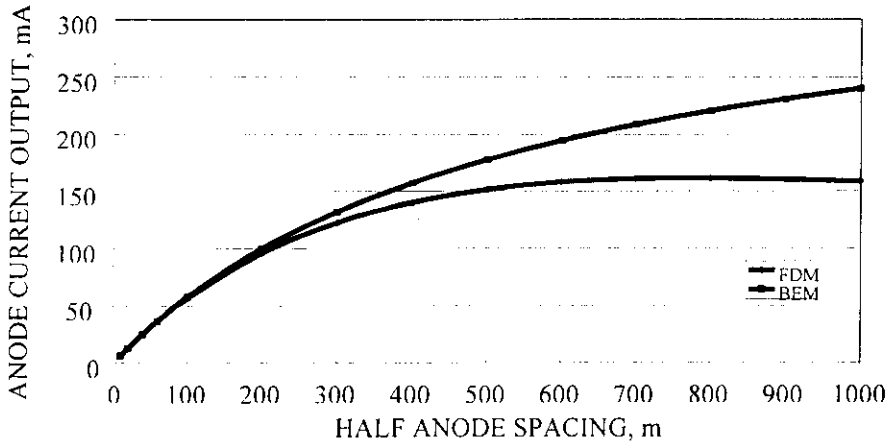

Figure 12: Anode current output, as projected by BEM and Equation 29 (FDM) as a function of half anode spacing and for $\alpha \cdot \gamma = 1{,}000\Omega \cdot m^2$.

and 10, where a more positive potential is projected by FDM than by BEM, correspond to the lower anode current outputs in Figures 11 and 12.

Figure 13 presents a plot of potential difference between the BEM and the FDM solution to Equation 29, as shown graphically in Figures 9 and 10, at the mid-anode location as a function of $\alpha \cdot \gamma$ and for various anode spacings from 50 to 10,000 m. This illustrates that, except for the shortest and greatest anode spacings (50 and 10,000 m, respectively), the difference between the two potentials increases with decreasing $\alpha \cdot \gamma$. This is a consequence of I_a increasing with decreasing $\alpha \cdot \gamma$ such that a correspondingly increasing voltage drop along the metallic path that was not accounted for in the BEM analysis resulted.

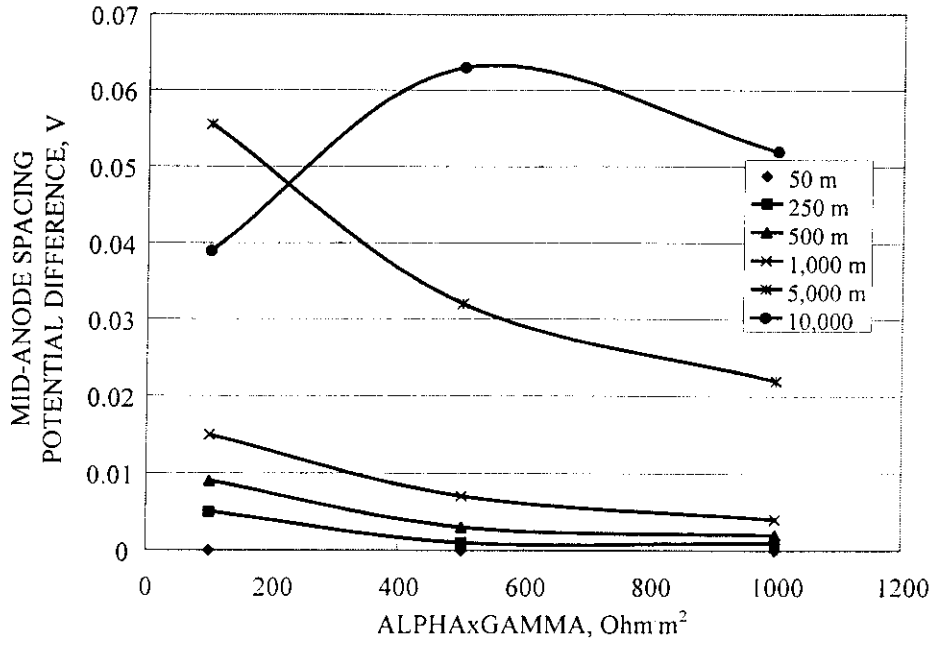

Figure 13: Plot of the difference between the FDM solution to Equation 29 and BEM projections of pipe potential at the mid-anode location for different anode spacings as a function of $\alpha \cdot \gamma$. The convention employed was that a positive difference indicates a more negative projected potential via BEM.

This trend was absent in the $2L$ = 50 m case because metallic path resistance is negligible for such a short anode spacing at the $\alpha \cdot \gamma$ values considered. A reverse trend resulted for $\alpha \cdot \gamma$ values below about 600 $\Omega \cdot m^2$ and $2L$ = 10,000 m. This apparently occurred because for these conditions polarization at the mid-anode location was relatively small in both the FDM and BEM cases, and so the potential difference between the two was small also.

Figure 14 presents a plot of the percent difference in anode current output as a function of $\alpha \cdot \gamma$ for the same $\alpha \cdot \gamma$ values and anode spacings as in Figure 13. For $2L$ values of 1,000 m and below, the difference is seen to be by less that six percent in all cases. However, for the two largest anode spacings, the I_a projected by BEM was significantly greater than for the FDM solution to Equation 29, particularly at low $\alpha \cdot \gamma$. In all cases, the difference increased with decreasing $\alpha \cdot \gamma$. This trend is consistent with those in Figures 11 and 12, where the I_a values projected by the two methods diverge with increasing $2L$ with the effect being greater the lower the $\alpha \cdot \gamma$.

The above examples illustrate the utility of an approach to pipeline cp design and analysis based upon an FDM solution to Equation 29 compared to already existing alternatives. Studies are presently underway

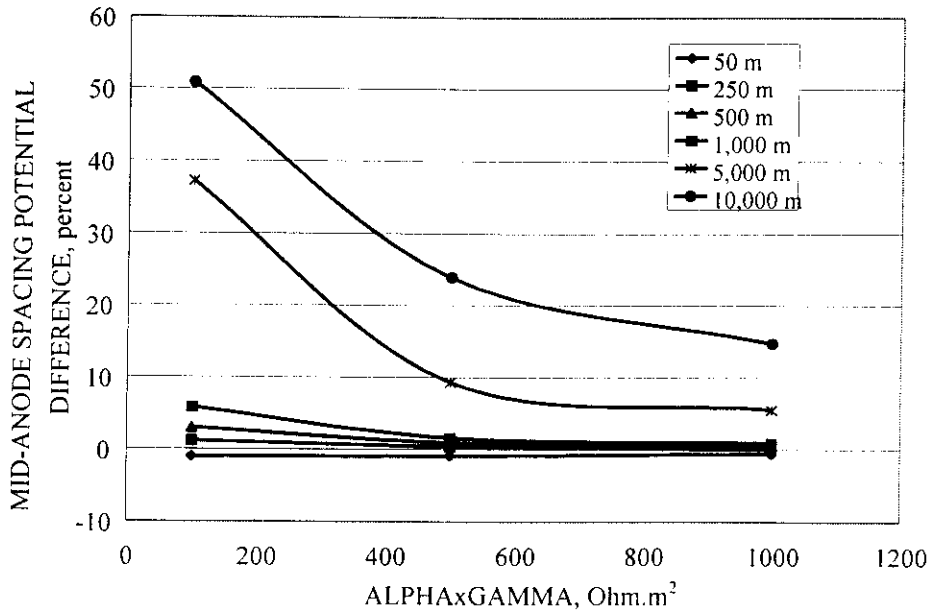

Figure 14: Plot of the percent difference in anode current output as projected by the FDM solution to Equation 29 and BEM for different anode spacings as a function of $\alpha \cdot \gamma$. The convention employed was that a positive difference indicates that BEM projected greater I_a.

to expand the applicability of Equation 29 to include situation of 1) anodes that are offset from the pipeline, 2) multiple grouped anodes, 3) multiple pipelines (parallel and crossing), 4) stratified electrolyte resistivity, and 5) different anode potentials.

Verification and Qualification of the Slope Parameter Design Method

Based upon Equation 29, a verification and qualification analysis was performed regarding accuracy of the Slope Parameter based method for pipeline cp design (Equations 21 and 23). Thus, Figure 15 shows the design ϕ_c for both the original (assumed length 0.209 m and radius 0.160 m) and final (80 percent depleted) anode sizes, the former being –0.975 $V_{Ag/AgCl}$ by choice (L_{as} was calculated using this value) and the latter – 0.943 $V_{Ag/AgCl}$ (determined by Equation 21 for ϕ_c based upon L_{as} = 170 m and the final anode dimensions). Also illustrated are the attenuation profiles from a FDM solution of Equation 29. The former are seen to be in good agreement with the latter except in the immediate vicinity of the anode, as should be expected. The metallic path resistance can be considered negligible for this anode spacing and $\alpha \cdot \gamma$ considered (100 $\Omega \cdot m^2$, since the trend demonstrated in Figures 9 and 10 (progressively more positive potential with increasing distance from an anode) is not seen in the FDM solutions in Figure 15. Anode current output was also determined 1) from the FDM solution to Equation 29 and 2) by resolving Equation 22 and recognizing that $i_m \cdot A_{c(1)} = I_a$ with the results being shown in Table 4. It is thought that the FDM solution to Equation 29 provided the more accurate result, in which case Equation 22 underestimated I_a by

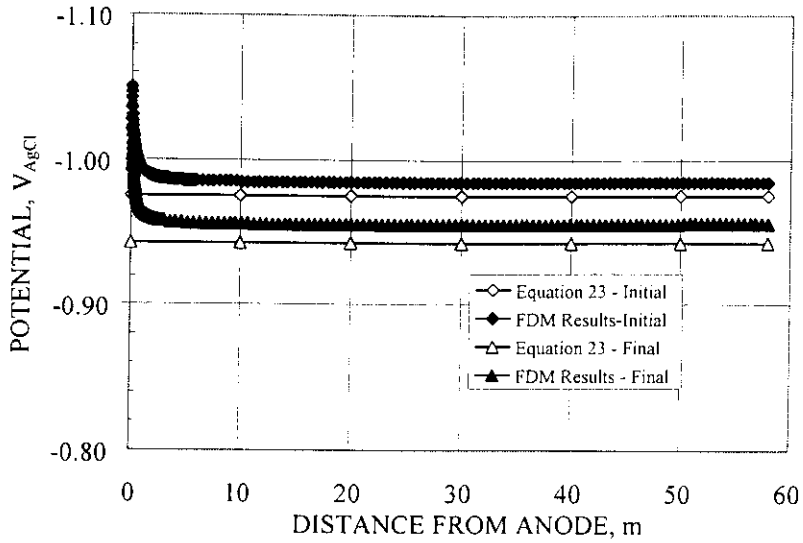

Figure 15: Comparison of the results from the FDM solution to Equation 29 with the cathode potential used in the cp design based upon Equation 23.

several percent. The difference is attributed to failure of Equations 20 and 21 to take into account the potential gradient near the anodes; however, this is thought to be within the uncertainty of the overall process and, hence, to be acceptable.

Table 4: Anode current output as determined using modifications to Equation 22 and the solution to Equation 29.

Condition	Anode Current Output, A		Difference,
	Equation 13	FDM Solution	%
Initial (Anode Weight 60.8 kg)	0.214	0.221	-3.1
Final (Anode Weight 12.3 kg)	0.193	0.202	-4.4

Range of Applicability of the Slope Parameter Design Approach

The proposed cp design approach based upon Equations 20 and 21 was evaluated by comparing the results from it with the corresponding FDM solution to Equation 29. Thus, Figure 16 presents a plot of the percent difference in ϕ_c at the mid-anode position (the location on the pipeline where polarization should be least) as a function of the corresponding $\alpha\gamma$ that results from application of Equation 21 compared to what is projected by the FDM solution to Equation 29 for the original anode and pipe dimensions in the above example using different values of L_{as}, and with ρ_c = 100 Ω·cm. Only data for which $\alpha\gamma \geq 30\ \Omega{\cdot}m^2$ and $\phi_c \leq$ -0.80 $V_{Ag/AgCl}$ are included. In all cases, the error is less than three percent, and so any design that includes the L_{as} and $\alpha\gamma$ values indicated here and which also satisfies Equation 22 or 23 is considered acceptable. Relatedly, Figure 17 plots anode current output error versus $\alpha\gamma$ for the same conditions as in Figure 16 where a negative error indicates greater current output per the FDM solution than what is projected by

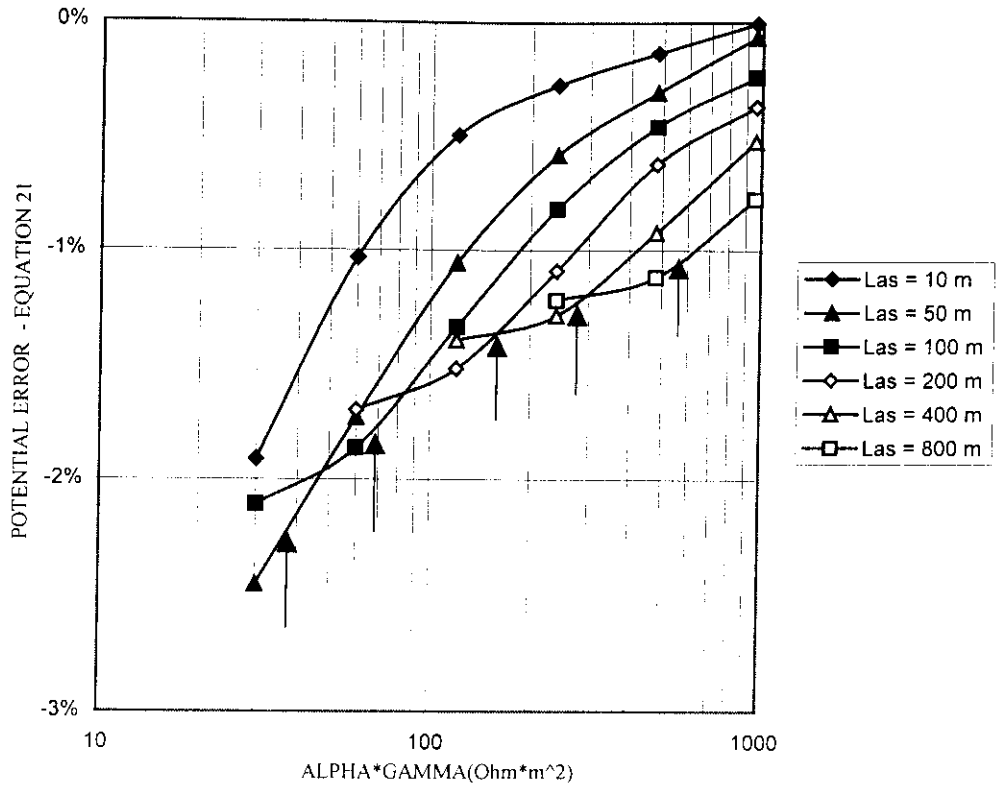

Figure 16: Error in polarized potential at the mid-anode position as determined from Equation 21 and referenced to the FDM solution to Equation 29 for ρ_e = 100 Ω.m.

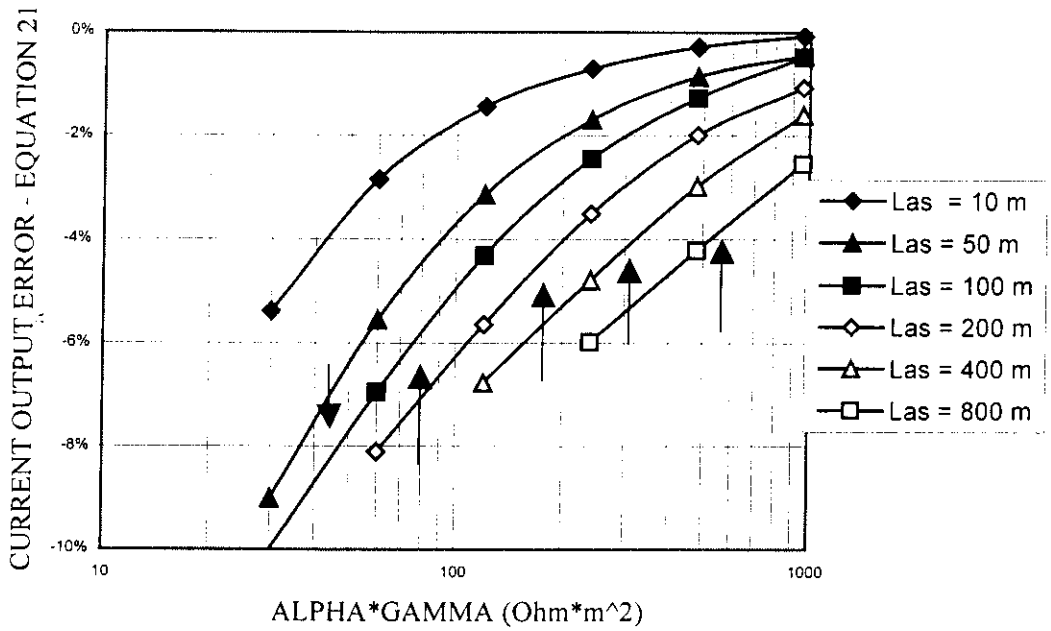

Figure 17: Error in anode current output as determined from a modified Equation 22 and referenced to the FDM solution to Equation 29 for ρ_e = 100 Ω.cm.

Equation 21. The percent error in current output at a particular $\alpha\gamma$ is greater than for potential (Figure 16) but is still considered acceptable for most engineering applications. Similarly, for the same design parameters but with a 15 Ω·cm electrolyte, the maximum mid-spacing potential and anode current output errors are –1.5 and –5.0 percent, respectively, which are less than for the 100 Ω·cm electrolyte. In the latter case, an additional calculation is necessary to confirm that adequate anode mass is available. Then by resolving Equation 23 using defined values for all other parameters (C = 1700 Ah/kg and u =0.8), the minimum acceptable $\alpha\gamma$ for anodes to achieve a 30 yr design life (that is, to maintain $\phi_c \leq$-0.80 $V_{Ag/AgCl}$) was determined. The results of this calculation, along with the corresponding ϕ_c values, as calculated iteratively using Equations 21 and 23, are listed in Table 5 and are indicated for each L_{as} in Figure 16 by an arrow (no arrow is shown for L_{as} = 10 m since the minimum $\alpha\gamma$ for this anode spacing is below 30 Ωm^2. In the high $\alpha\gamma$ regime, the errors are relatively small (the negative error indicates greater polarization according to the FDM solution compared to Equation 23), they converge with increasing $\alpha\gamma$, and order in proportion to anode spacing (larger error the greater the anode spacing). The proposed design method has the advantage of providing an iterative approach whereby different parameters, including anode spacing and cathode potential, can be optimized.

Table 5: Listing of the minimum allowable $\alpha \cdot \gamma$ and the corresponding resultant cathode potential to achieve a 30 yr design life using a 60.8 kg anode, on a 0.271 m diameter pipeline in 100 Ω·m seawater.

ANODE SPACING, m	MINIMUM ALLOWABLE ALPHA*GAMMA, $\Omega.m^2$	RESULTANT CATHODE POTENTIAL, $V_{Ag/AgCl}$
10	7	-0.910
50	35	-0.910
100	70	-0.910
200	141	-0.910
400	282	-0.910
800	565	-0.910

CONCLUDING REMARKS

The results to-date from this project are somewhat academic and are presently not in a useful format for the practicing engineer. In this regard, work is continuing with the ultimate goal of establishing criteria and a protocol for design of retrofit cp systems upon marine pipelines. It is intended that this will be provided in a spreadsheet format. Remaining issues that are to be addressed as a part of achieving this goal include the following:

1. Electrolyte resistivity stratification.
2. . Displaced rather than superimposed anodes.

3. Variable anode potentials.
4. Variable anode spacings.
5. Interpretation of survey data.
6. Protection extending from a platform.
7. Parallel pipes.
8. Crossing and joining pipes.

Efforts are also ongoing to expand the project to include industry participation. It is considered that only by doing this can the full potential of this research be realized.

BIBLIOGRAPHY

1. T. Andersen and A. Misund, "Pipeline Reliability: An Investigation of Pipeline Failure Characteristics and Analysis of Pipeline Failure Rates for Submarine and Cross-Country Pipelines," J. Pet. Technology, April, 1983, p. 709.

2. "Analysis of the MMS Pipeline Leaks Report for the Gulf of Mexico, Texaco USA, 133 W. Santa Clara, Ventura, CA 93001, October 25, 1985.

3. J. S. Mandke, "Corrosion Causes Most Pipeline Failures in the Gulf of Mexico, Oil and Gas Journal, October 29, 1990, p. 40.

4. C. Weldon and D. Kroon, "Corrosion Control Survey Methods for Offshore Pipelines," Proceedings International Workshop on Offshore Pipeline Safety, New Orleans, Dec. 4-6, 1991, p. 196.

5. Morgan, J., *Cathodic Protection*, Macmillan, New York, 1960, pp. 140-143.

6. Uhlig, H. H. and Revie, R. W., *Corrosion and Corrosion Control*, Third Edition, John Wiley and Sons, New York, 1985, p. 223.

7. "Cathodic Protection Design," *DnV Recommended Practice RP401*, Det Norske Veritas Industri Norge AS, 1993.

8. "Pipeline Cathodic Protection – Part 2: Cathodic Protection of Offshore Piipelines," Working Document ISO/TC 67/SC 2 NP 14489, International Standards Organization, May 1, 1999.

9. "Corrosion Control of Steel-Fixed Offshore Platforms Associated with Petroleum Production", *NACE Standard RP 0176*, NACE, Houston, 1976.

10. Wang, W., Hartt, W. H., and Chen, S., *Corrosion*, vol. 52, 1996, p. 419.

11. W. H. Hartt, Chen, S., and Townley, D. W., *Corrosion*, vol. 54, 1998, p 317.

12. Townley, D. W., "Unified Design Equation for Offshore Cathodic Protection," paper no. 97473 presented at CORROSION/97, March 9-14, 1997, New Orleans.

13. "Design of Galvanic Anode Cathodic Protection Systems for Offshore Structures," NACE International Publication 7L198, NACE International, Houston, TX, 1998.

14. Dwight, H. B., *Electrical Engineering*, Vol. 55, 1936, p. 1319.

15. Sunde, E. D., *Earth Conduction Effects in Transmission Systems*, Dover Publications, Inc., New York, 1968.

16. McCoy, J. E., *Transactions Institute of Marine Engineers*, Vol. 82, 1970, p. 210.

17. Cochran, J. C., "A Correlation of Anode-to-Electrolyte Resistance Equations Used in Cathodic Protection," paper no. 169 presented at CORROSION/82, March 22-26, 1982, Houston.

18. Strommen, R., *Materials Performance*, Vol. 24(3), 1985, p. 9.

19. Cochran, J. C., "Additional Anode-to-Electrolyte Resistance Equations Useful in Offshore Cathodic Protection," paper no. 254 presented at CORROSION/84, April 2-6, 1984, New Orleans.

20. Foster, T., and Moores, V. G., "Cathodic Protection Current Demand of Various Alloys in Sea Water," paper no. 295 presented at CORROSION/86, March 17-2, 1986, Houston.

21. Mollan, R. and Anderson, T. R., "Design of Cathodic Protection Systems," paper no. 286 presented at CORROSION/86, March 17-2, 1986, Houston.

22. Fischer, K. P., Sydberger, T. and Lye, R., "Field Testing of Deep Water Cathodic Protection on the Norwegian Continental Shelf," paper no. 67 presented at CORROSION/87, March 9-13, 1987, San Francisco.

23. Fischer, K. P. and Finnegan, J. E., "Cathodic Protection Behavior of Steel in Sea Water and the Protective Properties of the Calcareous Deposits," paper no. 582 presented at CORROSION/89, April 17-21, 1989, New Orleans.

24. Schrieber, C. F. and Reding, J., "Application Methods for Rapid Polarization of Offshore Structures," paper no. 381 presented at CORROSION/90, April 23-27, 1990, Las Vegas.

25. Mateer, M. W. and Kennelley, K. J., "Design of Platform Anode Retrofits Using Measured Structure Current Density", paper no. 526 presented at CORROSION/93, March 8-12, 1993, New Orleans.

26. Burk, J. D., "Dualnode Field Performance Evaluation – Cathodic Protection for Offshore Structures," paper no. 309 presented at CORROSION/91, March 11-14, 1991, Cincinnati.

27. McCoy, J. E., "Corrosion Control by Cathodic Protection – Theoretical and Design Concepts for Marine Applications", The Institute of Marine Engineers Transactions, Vol. 82, 1970, p. 210.

28. P. Pierson, K. Bethune, W. H. Hartt, and P. Anathakrishnan, "A New Equation for Potential Attenuation and Anode Current Output Projection for Cathodically Polarized Marine Pipelines and Risers," Corrosion, Vol. 56, 2000, p. 350.